Hindawi
International Journal of Antennas and Propagation
Volume 2024, Article ID 2048009, 8 pages
https://doi.org/10.1155/2024/2048009

Research Article

An EIRP Measurement Method of High-Power Microwave Systems Based on Near-Field Testing

Xianggang Hu [1,2] Jiancang Su,[2] Mingtao Zhang,[2] Xi Li [3] Dingkun Ma,[2] Jingang Gong,[2] Kewei Cheng,[2] Jia Liu,[2] Jiande Zhang,[1] Rui Li,[2] Jie Cheng,[2] and Shaotong Wu[2]

[1]*College of Advanced Interdisciplinary, National University of Defense Technology, Changsha 410073, China*
[2]*Key Laboratory of Advanced Science and Technology on High Power Microwave, Northwest Institute of Nuclear Technology, Xi'an 710024, China*
[3]*Key Laboratory of Antennas and Microwave Technology, Xidian University, Xi'an 710071, China*

Correspondence should be addressed to Xi Li; xli@xidian.edu.cn

Received 16 October 2023; Revised 2 January 2024; Accepted 30 January 2024; Published 7 February 2024

Academic Editor: Arpan Desai

The equivalent isotropic radiated power (EIRP) of high-power microwave (HPM) systems is a core-evaluating indicator. In practical testing, locating a suitable test site for the far-field method becomes challenging due to the requisite antenna separation. The conventional near-field method necessitates the extraction of the antenna's near-field distribution, resulting in a testing system of intricate complexity and diminished efficiency. Therefore, the traditional near-field method cannot be directly applied in HPM systems. In the present study, a new EIRP measurement method for HPM systems based on near-field testing was proposed. First, a monitoring antenna of a considerable scale is positioned within the near-field vicinity of the HPM antenna to capture radiation power, thereby deriving its equivalent input power. Subsequently, according to the EIRP definition and the measured gain of the HPM antenna, the EIRP of the HPM system can be acquired. Theoretical research on this measurement method was conducted, the electromagnetic simulation model was constructed, and a comprehensive analysis through simulation was undertaken. A measurement system was developed and verified experimentally. The results demonstrate the precision of this approach in determining the EIRP of the HPM system, thereby serving as a valuable tool for assessing the power-handling capability of the HPM antenna. The test error is ±0.5 dB.

1. Introduction

As high-power microwave (HPM) technology continues to develop, HPM systems have been widely applied in military, medical, energy, and other fields [1, 2]. In simple terms, an HPM system consists of primary power, pulsed power, an HPM source, and an HPM antenna [3–5]. To evaluate the overall performance of an HPM system, it is necessary to obtain the equivalent isotropic radiated power (EIRP). EIRP is normally used to restrict the amount of radiation power received from wireless equipment, which is defined as EIRP = $G_t \times P_t$, where G_t is the gain of the transmitting antenna and P_t represents its input power. There are three EIRP measurement methods: direct calculation, far-field [6–10], and near-field [11–16].

The direct calculation method, which is based on the definition of EIRP, cannot evaluate the power-handling capability and radiation characteristics of the HPM antenna. Thus, its application in HPM systems remains infrequent.

The far-field method involves testing the received power through a standard receiving antenna positioned in the far field of the antenna under test (AUT), and the system's EIRP is determined through path attenuation calculations. This method has been widely used in ground communication, satellite communication, radar detection, and various other fields. The test error associated with this method primarily stems from calibration inaccuracies within the measuring components and evaluation uncertainties concerning spatial attenuation and multipath interference caused by reflections from structures, trees, terrain, and other sources. The EIRP of an HPM system is usually calculated by the far-field method. Meanwhile, the assessment of the HPM antenna's power-handling capability and its radiation characteristics under HPM pulses involves a comparison of online and radiation waveforms. However, this method has two shortcomings: (i) It must satisfy the AUT's far-field condition. In the case of electrically large antennas, the far-field distance [17, 18] ranges from several kilometers to several hundred meters, posing challenges in locating appropriate test sites during practical testing. (ii) The method requires a receiving antenna to identify the far-field direction with the highest value of the AUT's radiation. During this calculation, any multipath interference at the testing site is disregarded. A larger test error may thus be produced.

The near-field method involves acquiring the amplitude and phase distribution of the electric or magnetic field through the controlled movement of a probe in the proximity of the AUT. By using the near-far field variation method, the far-field characteristics of the AUT are obtained, and subsequently enabling the calculation of the EIRP. In [12], a measurement method based on the Fresnel region was chosen to remove multipath interference. A straightforward phase-retrieval technique, enriched with a priori information, was introduced. This refinement allowed data acquisition to occur along a single line, eliminating the requirement for two-dimensional movement. Another paper [13] described an experimental method of characterizing the EIRP of electrically large antennas within a confined environment, obviating the need for separation between the generator and the radiating element. A near-far field variation method was used, wherein the phase was deduced through a comparison of signals received by both the reference antenna and the receiving antenna. This technique was suitable for the characterization of large-scale antennas within compact anechoic chambers. A study [14] proposed a methodology for EIRP system calculation employing the amplitude and phase distribution of the magnetic field within the AUT's very near-field region. The method had the advantages of a reduced scanning area and enhanced testing efficiency. Another study [15] proposed a coplanar phase-less near-field measurement system. By means of phase reconstruction, the electric field distribution on the far-field spherical surface of the AUT could be obtained. Subsequently, the near-far field variation method could be employed to ascertain the EIRP. These near-field methods simplified the testing process while enhancing precision. However, these methods required scanning within the AUT's near-field area and used the near-far field variation technique for EIRP determination. Due to the inherent characteristics of the HPM source, the output phase of each pulse exhibited instability, rendering the acquisition of near-field phase distribution unattainable through scanning. Therefore, the traditional near-field method cannot be applied directly in HPM systems.

In summary, traditional EIRP measurement methods cannot meet the requirements of high efficiency and precision within HPM systems, and their implementation within limited test sites remains unfeasible. Thus, new EIRP measurement methods need to be explored.

Here, a novel EIRP measurement method for HPM systems is proposed and carried out in the near-field region of the HPM antenna. Utilizing a large-scale monitoring antenna placed in the near-field region, radiation power is captured and the equivalent input power of the HPM antenna is computed. The EIRP of the HPM system is derived from the equivalent input power and gain of the HPM antenna. For verification, a simulation of an HPM system within an anechoic chamber is conducted, followed by a comprehensive discussion of the experimental findings.

Compared to the traditional near-field method, the new approach proposed in this paper offers several advantages: (1) It eliminates the need for near-far field transformation in electric field data, simplifying the calculation method. (2) The collection of phase information in the electric field is unnecessary, making the testing process more straightforward. (3) Obtaining the EIRP of the tested system requires only a single pulse, making it particularly suitable for HPM systems. Unlike the traditional near-field method, which relies on the microwave phase stability of the measured system, the HPM system experiences phase instability between pulses. Consequently, the traditional near-field method is unsuitable for application to HPM systems.

The paper is structured as follows: Section 2 elaborates on the method's principles, Section 3 delves into the design of the test system, Section 4 encompasses the execution of validation experiments along with result reporting, and ultimately, Section 5 presents our concluding insights.

It should be emphasized that the method proposed in this paper is applicable across various forms of HPM antennas. In order to illustrate and carry out the verification experiment, the HPM antenna used in this study takes the form of a double reflector.

2. Principles and Methods

The proposed method is illustrated in Figure 1. The HPM antenna is in the form of a double reflector, which consists of a main reflector, a subreflector, and a feed horn. A long-focus offset-feed reflector antenna (OFRA) was installed as a monitoring antenna in front of the HPM antenna.

The principle of the method is as follows: The separation between the OFRA and the HPM antenna is L. The aperture field of the HPM antenna is discretized with a discrete spacing of d on both the y and z axes, and the aperture field matrix is E_{mn}^{ap}. The electric field E_{uv}^{far} at the far-field region of the HPM antenna can be expressed as

$$E_{uv}^{\mathrm{far}} = \frac{1}{A} \cdot \sum_{m=1}^{M} \sum_{n=1}^{N} E_{mn}^{\mathrm{ap}} \exp\{jk \cdot \sin\theta \cdot (\mathrm{md}\cos\varphi + \mathrm{nd}\sin\varphi)\}, \tag{1}$$

in which A is a constant related to the wave amplitude, θ represents the pitch angle, and φ stands for the azimuthal angle. The terms md and nd correspond to the position within the aperture field that require discretization. U, v, m, and n are integers, which are the position coordinates of the discretized electric field. When angle θ is 0°, E_{uv}^{far} can be simplified to

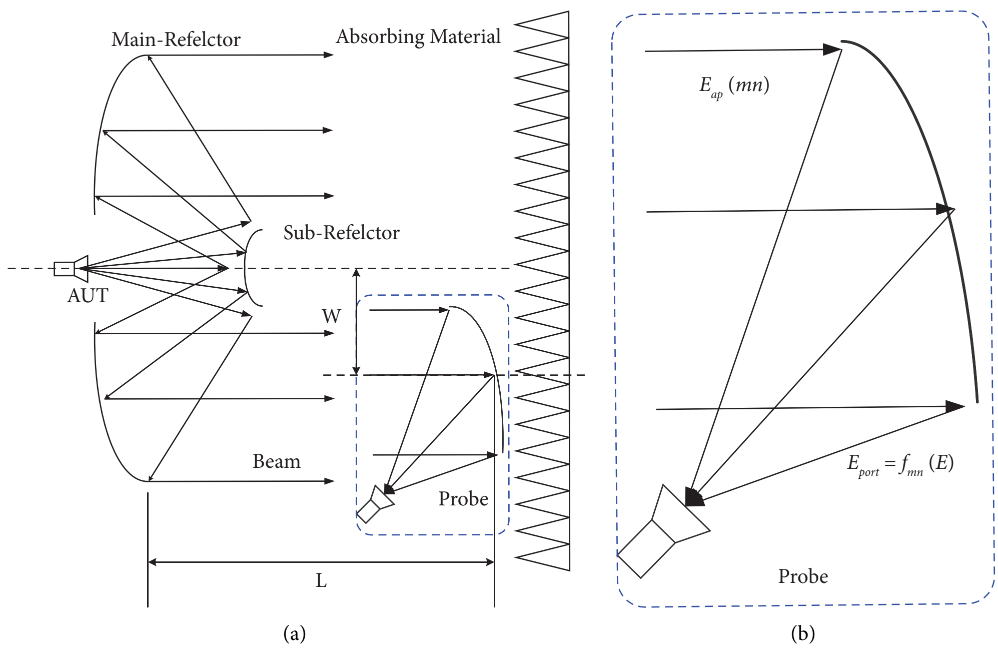

Figure 1: (a) Measurement method scheme and ray-tracing (b) monitoring antenna.

$$E_{uv}^{far}(\theta = 0^{\circ}) = \frac{1}{A}\sum_{m=1}^{M}\sum_{n=1}^{N} E_{mn}^{ap}. \quad (2)$$

In order to minimize the impact of scattered waves from the monitoring antenna on the radiation fields of the HPM antenna, the monitoring antenna is configured as an OFRA. When the aperture electric field $E_{ap}(m,n)$ is excited, the port response function E_{port} of the monitoring antenna can be expressed as

$$E_{port} = f_{mn}\left(E_{ap}(m,n)\right), \quad (3)$$

E_{port} is mainly determined by the radiation characteristics of the feed from the OFRA to the reflector. f_{mn} is used to represent the functional relationship between the E_{port} and $E_{ap}(m,n)$.

According to the theory of aperture antenna rays, we can assume $E_{ap}(m,n) = E_{mn}^{ap}$, so E_{port} can be shown as

$$E_{port} = \sum_{m=1}^{M}\sum_{n=1}^{N} f_{mn}\left(E_{mn}^{ap}\right). \quad (4)$$

Assuming that the feed of the OFRA irradiates the reflector with a constant amplitude, E_{port} can be calculated using the following expression:

$$E_{port} = \sum_{m=1}^{M}\sum_{n=1}^{N} B\cdot E_{mn}^{ap} = B\cdot A\cdot E_{uv}^{far}(\theta = 0^{\circ}), \quad (5)$$

where B is a constant related to the wave amplitude. Equation (5) gives the relationship between E_{uv}^{far} and E_{port}.

When the HPM antenna radiates HPM, the response function of the antenna's aperture field can be expressed as

$$E_{mn}^{ap} = \alpha_{mn}\cdot E_{mn}^{inc}\cdot \exp\left(j\varphi_{mn}\right), \quad (6)$$

in which E_{mn}^{inc} is the incident electric field and α_{mn} and φ_{mn} are the attenuation and phase shift constants, respectively, caused by the plasma, which is generated when the breakdown occurs as the antenna radiates HPMs.

Due to the varying electric field strengths produced by different antenna aperture positions, the resulting plasma effects also exhibit diversity, resulting in distinct values for α_{mn} and φ_{mn}. Under the low-power microwave (LPM) condition, the plasma effect does not occur, so $\alpha_{mn} = 1$ and $\varphi_{mn} = 0$. Therefore, the far field of the HPM antenna can be expressed as

$$E_{lowpower}^{far}(\theta = 0^{\circ}) = \frac{1}{A}\sum_{m=1}^{M}\sum_{n=1}^{N} E_{mn}^{inc} = \frac{1}{AB}E_{port}^{lowpower}, \quad (7)$$

in which $E_{port}^{lowpower}$ is the electric field strength of the feed of the OFRA with LPMs.

In the HPM condition, the far field of the HPM antenna can be given by

$$\mathrm{E}_{highpower}^{far}(\theta = 0^{\circ}) = \frac{1}{A}\sum_{m=1}^{M}\sum_{n=1}^{N}\alpha_{mn}E_{mn}^{inc}\cdot e^{j\varphi_{mn}} = \frac{1}{AB}E_{port}^{highpower}, \quad (8)$$

in which $E_{port}^{highpower}$ is the electric field strength of the feed of the OFRA. In Equations (7) and (8), the far-field characteristics of the HPM antenna can be ascertained through the utilization of the electric field at the feed port of the OFRA.

Based on the above principles, the test system can be simplified to a two-port model, as shown in Figure 2.

In Figure 2, Port 1 is the microwave input port of the HPM antenna and Port 2 is the microwave output port of the monitoring antenna. S_{21} is the transmission coefficient of the test system, which not only reflects the coupling relationship between Ports 1 and 2 but also evaluates the influence of the

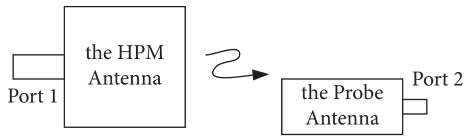

Figure 2: Test system equivalent model.

test environment and the nonlinear effect. S_{21} is used to evaluate the power transmission and is equivalent to $1/AB$ in (7).

Given the linearity of free-space microwave transmissions, the stability of S_{21} is achieved when the antennas maintain a consistent positional relationship, ensuring that the HPM antenna's test environment and performance remain unchanged. Hence, S_{21} can be used to assess the nonlinear effects of the HPM antenna under HPM. If the received power of S_{21} and Port 2 under HPM are known, the equivalent input power can be acquired at Port 1. Therefore, the EIRP of the HPM system can be achieved by combining the test gain of the HPM antenna. In the actual test, S_{21} can be tested under LPM, and the received power of Port 2 under HPM can be obtained, so the EIRP can be easily calculated.

While confirming the separation between the monitoring and HPM antennas on the one hand and the size of the monitoring antennas on the other, three main factors can be considered: (i) The monitoring antenna exhibited minimal alteration to the HPM antenna's near-field distribution. Given the limitations of the test environment, the separation could not be excessively distant. (ii) The presence of scattered waves from the monitoring antenna did not significantly disrupt the HPM antenna's near-field distribution. Therefore, absorbing materials were strategically placed around the monitoring antenna to attenuate and mitigate the impact of these scattered waves on the near-field distribution. (iii) The dimensions of the monitoring antenna must be chosen judiciously; a large size presents challenges in attainment, while a smaller size could result in substantial testing errors.

For these reasons, the simulation model was established in the Ku band, as shown in Figure 3. The HPM antenna is a dual-reflector antenna, and the diameter D of the main reflector is 3.0 m. The monitoring antenna is the OFRA, and the diameter of the reflector is 1.5 m. Antenna separation L is 5.0 m, and the axis distance W in the horizontal direction of the reflector is 0.75 m.

Figure 4(a) illustrates the simulation model of the OFRA within the electromagnetic simulation software, while Figure 4(b) depicts its radiation pattern. The gain at the centre frequency of the OFRA is 45.4 dBi, with a corresponding 3 dB beamwidth of approximately 0.80°.

After completing the design of the OFRA, an integrated simulation is carried out with the HPM antenna. Disregarding the ohmic losses of the antennas and the influence of the test environment, the theoretically calculated value for the parameter S_{21} is −8.63 dB. In the actual test, S_{21} is subjected to the calibration result from LPM measurements.

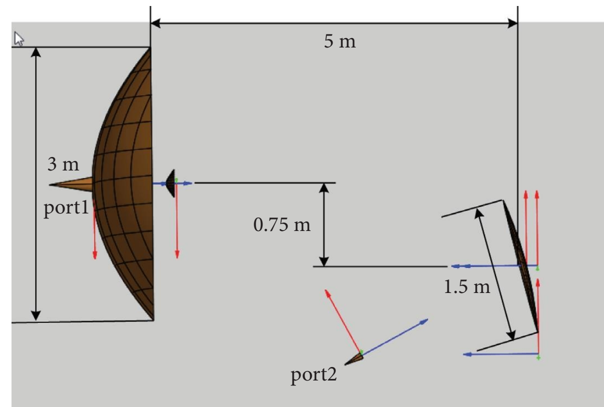

Figure 3: Test system simulation model (top view).

To assess the method's effectiveness, the test error is simulated based on the normal state simulation. A ring groove is opened on the main reflector of the HPM antenna to simulate an abnormal state in the antenna performance, as shown in Figure 5. The directivity (D) of the HPM antenna decreases as the size of the ring groove increases, leading to a reduction in S_{21} within the test system. The test error of this method can be obtained by comparing ΔD and ΔS_{21}. As observed in Table 1, ΔS_{21} varies with the change in ΔD, and the evaluation of ΔD can be assessed through the corresponding values of ΔS_{21}. When the variation in ΔD is below 0.7 dB, the error in evaluating ΔS_{21} is less than 0.2 dB.

3. Test System

The configuration of the test system is shown in Figure 6. The test system consists of an OFRA, measurement components, support and adjustment platforms, and absorbent materials.

The OFRA, which is shown in Figure 7, consists of an offset reflector and a feed horn. The offset reflector, with a diameter of 1.5 m and a focal distance F of 2.36 m, was placed in front of the HPM antenna at a distance of 5.0 m. The axes of the two reflectors were aligned at an identical height, maintaining a horizontal distance of 0.75 meters between them. The feed horn employed was a multimode, variable-angle horn, with its phase center located at the focal point of the offset reflector. The measurement components, shown in Figure 8, included a mode converter, an online coupler, a high-power absorbing load, and a detector. The support-adjustment platforms were used to improve the accuracy of the measurement system. The OFRA and measurement components were placed on the support-adjustment platforms capable of five-dimensional adjustments. These adjustments ensured the precise alignment of the offset reflector, feed horn, and main reflector in their relative positional relationship.

The measurement components were in the form of aluminum circular waveguides with diameters of 30 mm. The simulation results indicate that with an injection power of 1 GW, the maximum field strength within the waveguide reaches around 600 kV/cm. This value remains below the breakdown threshold of aluminum under vacuum pressure. Therefore, the power-handling capability of the measurement

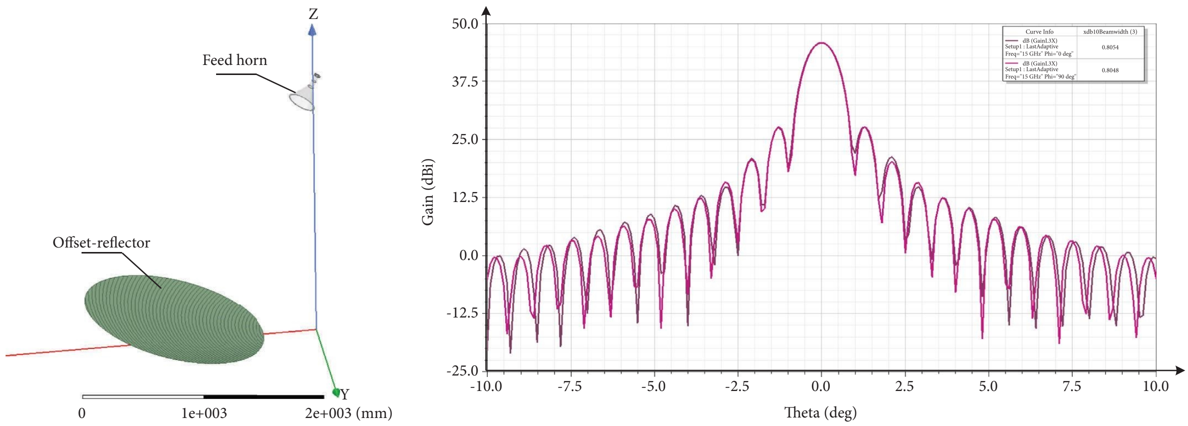

(a) (b)

Figure 4: (a) The OFRA simulation model. (b) The OFRA radiation pattern.

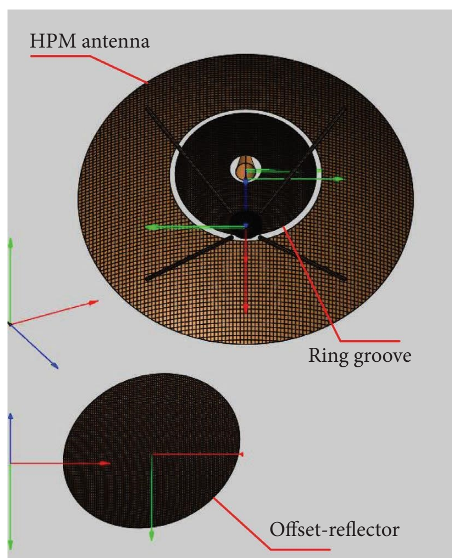

Figure 5: Simulation model of HPM antenna-opening ring groove.

Table 1: S_{21} changes with the width of the ring groove.

	Ring width (mm)			
	0	25	50	100
D (dBi)	51.77	51.60	51.42	51.06
ΔD (dB)	0	−0.17	−0.35	−0.71
S_{21} (dB)	−8.63	−8.84	−9.06	−9.52
ΔS_{21} (dB)	0	−0.21	−0.43	−0.89
$\Delta S_{21} - \Delta D$ (dB)	0	0.04	0.08	0.18

component exceeds 1 GW. The results show that the breakdown threshold of air under normal pressure is approximately 30 kV/cm. According to the working characteristics of the HPM system, the radiation field of the HPM antenna generally remains below 30 kV/cm. The offset reflector was made of aluminum, with a breakdown threshold significantly surpassing 30 kV/cm. As a result, its power-handling capability adequately meets the test requirements.

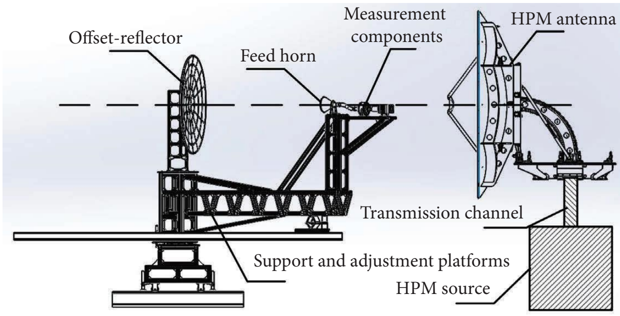

Figure 6: Test system configuration (side view).

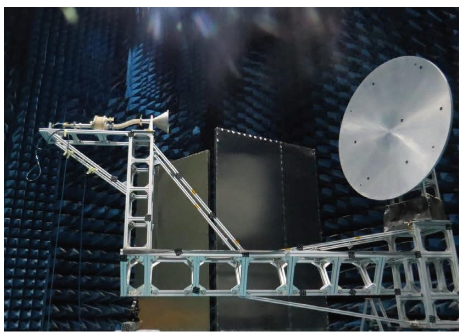

Figure 7: OFRA.

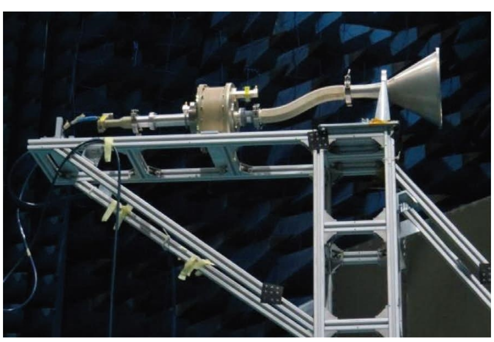

Figure 8: Measurement components.

4. Experiments and Results

The test system was meticulously developed, and subsequent verification experiments were carried out within the testing facility. The test procedure was as follows:

(i) We established the test system according to the positional relationship between the HPM and the monitoring antennas. The main and offset reflectors must meet the following positional relationship: $L = 5.0\,m \pm 2$ mm, $W = 0.75\,m \pm 1$ mm, an axis height deviation of less than 1 mm, a pitch angle deviation of less than 0.05°, and an azimuth angle deviation of less than 0.05°. The offset reflector and the feed horn must meet the following positional relationship: $F = 2.36\,m \pm 0.5$ mm, an axis height deviation of less than 0.5 mm, a pitch angle deviation of less than 0.03°, and an azimuth angle deviation of less than 0.03°.

(ii) Prior to EIRP testing, it is essential to calibrate the parameter S_{21} of the test system under LPM conditions. S_{21} remains stable as long as both the HPM antenna and the test environment remain unchanged. Consequently, the calibration of S_{21} needs to be performed only once.

(iii) Following the positional calibration, we connected the test components and used the vector network analyzer to calibrate the parameter S_{21} of the test system. The measured value of S_{21} was −9.5 dB, exhibiting a deviation of −1 dB from the simulated result. This disparity was mainly attributed to the transmission loss within the test system.

(iv) During the operation of the HPM system, the HPM was radiated through the HPM antenna. The offset reflector intercepted the HPM, reflecting and concentrating it onto the feed horn. The received power of the feed horn was represented by P_2.

(v) The EIRP of the HPM system can be given by

$$\mathrm{EIRP} = P_2 + |S_{21}| + G_0\,(\mathrm{dBW}), \tag{9}$$

in which G_0 was the measured gain of the HPM antenna at LPM conditions.

In our validation test, P_2 was 80.1 dBW, G_0 was 50.2 dBi, and S_{21} was −9.5 dB. The EIPR of the HPM system was calculated as 139.8 dBW, using (9).

The primary source of the test error originated from the P_2 and S_{21} errors. The errors caused by the test environment were eliminated in the calibration process. In accordance with the general error analysis of the power test method, this method exhibits an error margin of approximately 0.5 dB. The EIRP obtained by this method represents the actual value of the HPM system during HPM radiation, accounting for the ohmic loss occurring during transmission and radiation of HPM, alongside the nonlinearity loss caused by the reflector breakdown. This result represents the most realistic and accurate assessment of HPM systems.

The output power of the HPM source used in the experiment is 89.9 dBW. By the definition of EIRP, the EIRP of the HPM system is calculated as 140.1 dBW. The EIRP measured by the proposed method in this paper is 139.8 dBW, showing a decrease of 0.3 dB, which falls within the allowable error range of the test. Another potential explanation for the observed decrease in EIRP could be attributed to microdischarges occurring in certain areas of the transmission path when the HPM antenna radiates. This phenomenon may lead to a slight increase in transmission loss, contributing to the reduction in EIRP.

By comparing the online waveforms of the HPM system with the waveforms received by the feed horn, it becomes possible to analyze the power-handling capability of the HPM antenna. If these two waveform types are the same, it indicates that the power-handling capability of the HPM antenna meets the stipulated criteria. The single-pulse waveforms of the HPM system and the OFRA are shown in Figure 9(a). In addition, Figure 9(b) displays the test waveform for a sequence of 10 Hz/1000

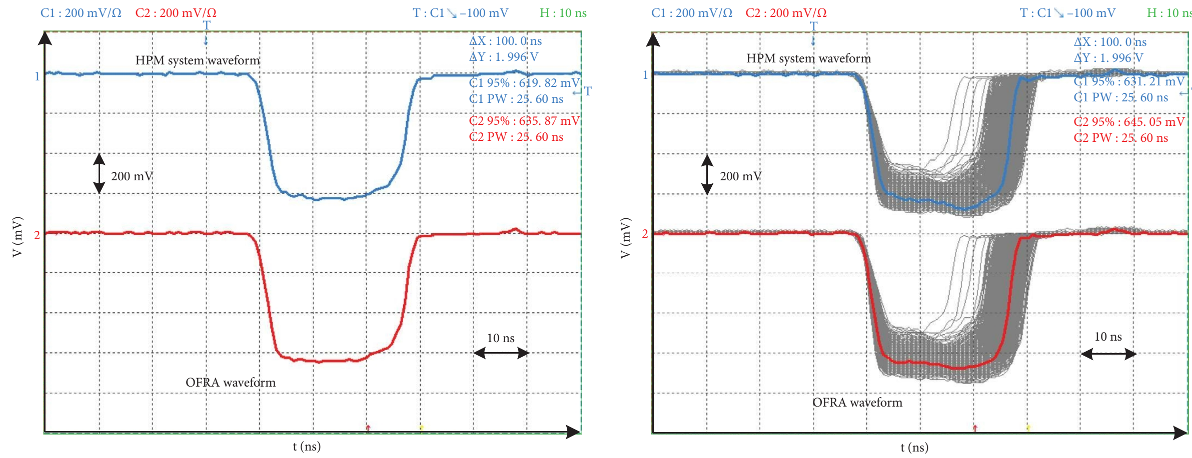

(a) (b)

FIGURE 9: (a) Test waveforms of a single pulse under HPM. (b) Test waveforms of 1000 pulses under HPM.

pulses. The two waveforms are completely consistent, indicating the absence of any breakdown within the HPM system.

5. Conclusions

This paper proposes a new EIRP testing approach tailored for HPM systems. This method not only circumvents the stringent constraints imposed by conventional testing methods concerning distance and environmental conditions but also mitigates test errors stemming from multipath effects. By offering high testing precision, robust environmental adaptability, and enhanced concealment, this method presents a fresh avenue for EIRP testing in HPM systems. Given the diverse applications of HPM systems, the presented testing method holds promise for further development and widespread adoption.

Data Availability

The data used to support the findings of this study are included within the article.

Conflicts of Interest

The authors declare that there are no conflicts of interest regarding the publication of this paper.

References

[1] J. Benford, J. A. Swegle, and E. Schamiloglu, "High power microwave applications," in *High Power Microwaves*, pp. 16–39, Taylor & Francis Group, New York, NY, USA, third edition, 2007.

[2] K. Chen and X. Zhou, "Development of high-power microwave technology," in *Proceedings of the 2019 IEEE 3rd Information Technology, Networking, Electronic and Automation Control Conference (ITNEC)*, pp. 2148–2152, Chengdu, China, March 2019.

[3] X. Li, Q. Liu, X. Wu, L. Zhao, J. Zhang, and Z. Zhang, "A GW level high-power radial line helical array antenna," *IEEE Transactions on Antennas and Propagation*, vol. 56, no. 9, pp. 2943–2948, 2008.

[4] R. A. Koslover and Tustin, "Compact, lightweight, steerable, high-power microwave antenna," U.S. Patent 6 559 807 B2, 2002.

[5] T. Liang, W. Hua, H. Shao, K. Wang, J. Li, and H. Huang, "Design and near field characteristic of high-power microwave dual-reflector antenna," in *Proceedings of the 2012 International Conference on Microwave and Millimeter Wave Technology (ICMMT)*, Shenzhen, China, May 2012.

[6] X. Li, G. Niu, B. Zhao, and L. Yang, "Single-cut far-field pattern determination of polarized linear antenna array via quasi-far-field mathematical absorber reflection suppression," *IEEE Transactions on Antennas and Propagation*, vol. 71, no. 3, pp. 2778–2783, 2023.

[7] X. Li, G. Wei, L. Yang, and B. Liao, "Fast determination of single-cut far-field pattern of base station antenna at a quasi-far-field distance," *IEEE Transactions on Antennas and Propagation*, vol. 68, no. 5, pp. 3989–3996, 2020.

[8] W. Zhang, Y. Zhong, L. Guo, S. Li, and Q. Wang, "Research on measurement method of electromagnetic wave equivalent radiation power," *Electronics Test*, vol. 3, pp. 68–71, 2022.

[9] F. Zhang, Z. Tian, and S. Liu, "Study on test method of equivalent radiated power," *Radio Engineering of China*, vol. 36, no. 4, pp. 47–49, 2006.

[10] J. Wang and S. Qin, "Measurement and error analysis of EIRP for active phased-array antenna," *Modern Electronics Technique*, vol. 37, no. 17, pp. 72-73, 2014.

[11] D. W. Hess, "Measurement of EIRP and antenna response for active antennas with spherical near-field scanning," in *Proceedings of the 2004 IEE Antenna Measurements and SAR, AMS 2004*, pp. 49–54, Loughborough, UK, May 2004.

[12] S. S. Oh and Y. H. Lee, "An EIRP measurement method for base-station antennas using field strengths measured along a single straight line," *International Journal of Antennas and Propagation*, vol. 2013, no. 1, Article ID 742636, 6 pages, 2013.

[13] S. S. Oh, W. Kim, and Y. Lee, "EIRP characterization of electrically large wireless equipment with integrated signal generator in a compact environment," *International Journal of Antennas and Propagation*, vol. 2015, no. 1, Article ID 383925, 5 pages, 2015.

[14] R. Ji, F. Zhou, L. Wang et al., "A roadside unit EIRP measurement method based on very near field scanning," in

Proceedings of the 2021 IEEE 21st International Conference on Communication Technology (ICCT), pp. 1068–1071, Tianjin, China, October 2021.

[15] K. Kyosuke and A. Hiroyuki, "Near field co-planar phase-less measurement for EIRP evaluation," in *Proceedings of the 2020 International Symposium on Antennas and Propagation (ISAP)*, pp. 331-332, Osaka, Japan, January 2021.

[16] X. Li, T. Zhang, M. Wei, and L. Yang, "Reduction of truncation errors in planar near-field antenna measurements using improved gerchberg–papoulis algorithm," *IEEE Transactions on Instrumentation and Measurement*, vol. 69, no. 9, pp. 5972–5974, 2020.

[17] A. J. V. D. Biggelaar, A. B. Smolders, and U. Johannsen, "Method to experimentally verify far-field conditions in a direct far-field measurement setup," in *Proceedings of the 2021 Antenna Measurement Techniques Association Symposium (AMTA)*, Daytona Beach, FL, USA, October 2021.

[18] K. T. Selvan and R. Janaswamy, "Fraunhofer and fresnel distances: unified derivation for aperture antennas," *IEEE Antennas and Propagation Magazine*, vol. 59, no. 4, pp. 12–15, 2017.